NASA TN D-860

Copy 1

TECHNICAL NOTE

D-860

PREDICTED SHOCK ENVELOPES ABOUT TWO TYPES OF VEHICLES AT LARGE ANGLES OF ATTACK

By George E. Kaattari

Ames Research Center
Moffett Field, Calif.

LIBRARY COPY

APR 28 1961

SPACE FLIGHT
LANGLEY FIELD, VIRGINIA

NATIONAL AERONAUTICS AND SPACE ADMINISTRATION

WASHINGTON April 1961

NATIONAL AERONAUTICS AND SPACE ADMINISTRATION

TECHNICAL NOTE D-860

PREDICTED SHOCK ENVELOPES ABOUT TWO TYPES OF VEHICLES AT LARGE ANGLES OF ATTACK

By George E. Kaattari

SUMMARY

Methods based on oblique- and normal-shock relationships and the continuity of mass flow through suitably chosen volume elements between the shock and body were developed to predict shock envelopes about two types of vehicles being considered for atmosphere entry. One type is a high-drag capsule shape. The other type is essentially a slender triangular wing capable of providing high lift or high drag, depending on the angle of attack. Predicted and measured shock envelopes were compared for a Mach number range of 3 to 15 for vehicles at high angles of attack; good agreement was found. Most of the available experimental data were in a speed and temperature range in which no important real-gas effects occurred.

INTRODUCTION

During atmosphere entry, a vehicle is exposed to aerodynamic forces and heating rates which are related to the strength and disposition of the shock envelope about the vehicle. Present methods (e.g., refs. 1 through 4) for defining detached shock envelopes are generally limited to simple shapes at zero or low angles of attack. Little information is available on predicting shock envelopes in the case of vehicles at high angles of attack.

The purpose of this paper is to present methods for defining shock envelopes for the case of high angle of attack and to present a comparison of predicted results of the analysis with experimental results. Two types of vehicles, shown in figure 1, are considered. The vehicle on the left is a high-drag capsule shape, capable of providing low lift-drag ratios over a limited angle-of-attack range. The vehicle on the right is essentially a slender wing capable of providing low drag and high lift-drag ratios, and high drag and low lift-drag ratios, depending upon the angle of attack. These two types of vehicles will hereinafter be called capsule and conical types, respectively.

METHODS

This section of the report will describe the general principles, relationships, and assumptions used in developing equations for predicting shock envelopes about capsule and conical types of vehicles; will present the derived equations; and will present the procedures and charts for applying the equations. Appendix A describes the symbols used. The detailed derivations of the equations are given in appendix B.

Common to the analyses for both types of vehicles was the application of (1) the continuity of mass flow between the shock wave and the vehicle surface, (2) oblique- and normal-shock relationships, and (3) the unique correlation of stagnation-point velocity gradient with Mach number for different bodies which was pointed out in reference 1. The analysis follows that of Moeckel in the utilization of items (1) and (2). The analysis differs in that the sonic line is not involved except in its terminal position on the body and in that the shock is assumed circular in shape rather than hyperbolic. The circular shock is adopted in the interest of generality since it is a simple compromise between the "hyperbolic-like" shock about cylinders or spheres and the "elliptic-like" shocks about long plates or discs. Moreover the shock dimension is then characterized by a single value R thus simplifying the analysis. Application of item (3) gives a means of determining the value for R as will be shown. The gas properties required in these applications were taken to be those of perfect gases or real gases in equilibrium. The analyses for the two types of vehicles differ as to detail and thus are described separately in the following two sections.

Capsule-Type Vehicles

Figure 2 illustrates the mass-flow components that are taken into account in the analysis of capsule-type vehicles. It is assumed that the shock wave is composed of circular-arc elements whose radii and location with respect to the body are to be determined. The sonic-point locations on the body are based on experimental and theoretical results (e.g., ref. 2) which indicate that for spheres, sonic points exist at surface elements inclined at about 45° to the stagnation streamline. In cases for which the spherical segment ends before the surface inclination attains 45°, the sonic point exists at the edges of the body.

The foregoing considerations and the application of mass-flow continuity resulted in the following equations:

$$\frac{\Delta}{R} = \frac{\sin\theta}{\frac{1}{2}\left(\frac{\rho_\theta}{\rho_o} - 1\right)\sin 2\theta + \frac{\rho_* V_*}{\rho_o V_o}\cos\varphi} \tag{1}$$

$$\frac{\Delta}{R} = \frac{\Delta_o}{R} + \frac{r}{R}(1 - \cos\varphi) - (1 - \cos\theta) \tag{2}$$

Equation (1) relates the ratio of the sonic-point shock standoff distance to shock radius, Δ/R, to the shock angular position θ opposite the sonic point, the density ratio across the shock at that position, ρ_θ/ρ_o, and the ratio of the mass flow per unit area at the sonic point, $\rho_* V_*$, to entering mass flow per unit area $\rho_o V_o$. Equation (2) is a geometric identity relating the sonic standoff distance to the standoff distance at the stagnation point, the body radius, r, and angular position of the sonic point, φ, and the shock radius and angular position, θ, opposite the sonic point. This equation is strictly applicable only to the axially symmetric case. In the general case, involving angle of attack, the stagnation streamline is curved and the expression relating Δ and Δ_o is more complex than equation (2). For many cases, however, the curvature is small so that length Δ_o is substantially the same as its horizontal projection. The approximation is made, therefore, that equation (2) is applicable to the general case.

The foregoing equations based on continuity and geometric relationships are not sufficient for a solution of shock-wave shape and location, because of the existence of three unknowns, Δ, R, and θ, and only two equations. The remaining quantities are either known (r, φ), calculable independently of the unknowns ($\rho_* V_*/\rho_o V_o$), or calculable as functions of the unknowns (Δ_o, ρ_θ/ρ_o). An independent equation giving additional relationships among the shock parameters is therefore needed. The third equation was derived on the basis of the previously mentioned velocity gradient correlation. The equation that follows defines a function which correlates the standoff distance at the stagnation point, the body stagnation point and shock radii, and the density ratio for various axisymmetric shapes:

$$f = 2\frac{\rho_o}{\rho_s}\left[1 - \left(1 + \frac{\Delta_o}{r}\right)\left(\frac{\rho_1}{\rho_o} - 1\right)\frac{\Delta_o}{R}\right] \tag{3}$$

The values of the correlation function f as a function of density ratio are shown in figure 3. The recommended values indicated were obtained from the derived correlation formula by using theoretical stagnation point standoff distances and shock radii given in reference 2 for spheres.

To define the shock radius and shock location, the three equations are solved simultaneously. For a solution it is necessary to relate ρ_θ/ρ_o with ρ_1/ρ_o and θ in equation (1). This relationship depends on the nature of the gas involved. For a perfect gas, ρ_θ/ρ_o can be expressed as a function of θ and ρ_1/ρ_o. The latter ratio and the other flow parameters, $\rho_* V_*/\rho_o V_o$ and ρ_s/ρ_o, can be calculated from perfect-gas relations. In the case of a real gas, charts or tables of the thermodynamic properties and normal-shock properties are required (refs. 5 and 6, respectively, in the case of air).

As a convenience in obtaining solutions of shock envelopes for the case of real air, the charts of figure 4 were prepared. These charts present values of Δ/R and θ as functions of the normal-shock density ratio, ρ_1/ρ_o, and φ. The application of these charts in determining the shock envelope is as follows: Consider the case of a vehicle at angle of attack, as shown in figure 2. We will confine our attention to the trace of the shock envelope on the vehicle's vertical plane of symmetry. These segments have radii R_1 and R_2 which coincide tangentially at the origin of the coordinate system X-Y. To locate the body with respect to these shock segments, the coordinates of the two sonic points (1) and (2) as well as the shock radii must be found. These values are given by the following equations:

$$\left.\begin{aligned}
X_1 &= \frac{|Y_2| + |Y_1| - (X_2 - X_1)\left[\dfrac{\sin\theta_2}{(\Delta/R)_2 + (1 - \cos\theta_2)}\right]}{\dfrac{\sin\theta_1}{(\Delta/R)_1 + (1 - \cos\theta_1)} + \dfrac{\sin\theta_2}{(\Delta/R)_2 + (1 - \cos\theta_2)}} \\
Y_1 &= \frac{X_1 \sin\theta_1}{\left(\dfrac{\Delta}{R}\right)_1 + (1 - \cos\theta_1)} \\
Y_2 &= |Y_2| + |Y_1| - Y_1 \\
R_1 &= \frac{Y_1}{\sin\theta_1} \\
R_2 &= \frac{Y_2}{\sin\theta_2}
\end{aligned}\right\} \quad (4)$$

The values of θ and Δ/R are located from the charts of figure 4 at the appropriate values of shock density ratio ρ_1/ρ_o and sonic-point inclination φ. The values $(X_2 - X_1)$ and $|Y_2| + |Y_1|$ are the known distances between the sonic-point coordinates (1) and (2). An example calculation is given in appendix B.

In preparing the charts presented in figure 4, the following three approximations were made: (1) for a value of ρ_1/ρ_o greater than 5, the value of ρ_θ/ρ_o was assumed to be equal to ρ_1/ρ_o; (2) the value of $\rho_* V_*/\rho_o V_o$ was always assumed to be equal to that given by the perfect-gas relations with $\gamma = 1.4$ (eq. (B1)); and (3) the value of ρ_s/ρ_o was always assumed to be that given by the perfect-gas relations with $\gamma = 1.4$ (eq. (B7)). The possible errors introduced by these approximations were assessed in the following manner.

Real-gas effects on ρ_s/ρ_o and $\rho_* V_*/\rho_o V_o$ were assessed by comparing the ideal-gas values (see eqs. (B1) and (B7)) with the values for equilibrium flow as calculated with the aid of the charts of reference 6 at various levels of density ratio, pressure, and enthalpy. It was found that no large differences existed between the values representing ideal and real gases. Small differences can be expected because of the weak dependence of $\rho_* V_*/\rho_o V_o$ and ρ_o/ρ_s on the specific heat ratio γ. In view of the foregoing, significant errors in the calculated shock dimensions then can arise only through the effects of large departures of the actual ratio ρ_θ/ρ_o from idealized conditions. To assess such errors, this effect of a real gas on the shock parameters θ, Δ, and Δ_o was evaluated. Values of these parameters for a sphere in air in equilibrium flow at a velocity and absolute density at which a large variation in ρ_θ/ρ_o occurs were compared with values obtained in a hypothetical gas having the same normal shock density ratio but with ρ_θ/ρ_o independent of θ. The calculated differences in Δ_o were negligible, but a small effect on shock radius resulted in a difference of about 15 percent in Δ between air in equilibrium and the hypothetical gas.

Conical-Type Vehicles

Figure 5 illustrates the mass-flow components that are taken into account for vehicles of conical type. Free-stream mass-flow components exist both in a crossflow direction ($\rho_o V_o \sin \alpha'$) and in a tangential direction ($\rho_o V_o \cos \alpha'$) as indicated. The shock-wave trace in the crossflow plane is taken as an arc of a circle. Sonic locations on the body are assumed to exist at points where the body surface inclination with the crossflow plane is 45°, for all finite ratios of a/b, and at the edge for the case of a flat plate ($a/b = 0$). For an infinitely slender elliptic cone, the determination of the shock envelope is essentially a two-dimensional (crossflow) problem. The shock dimensions in such a case are determined by the following equations which are analogous to equations (1) to (3).

$$\frac{\Delta}{R} = \frac{2 \sin \theta}{\frac{1}{2}\left(\frac{\rho_\theta}{\rho_o} - 1\right) \sin 2\theta + \frac{\rho_* V_*}{\rho_o V_o} \cos \varphi} \tag{5}$$

$$\frac{\Delta}{R} = \frac{\Delta_o}{R} + \frac{a}{R}\left[1 - \frac{a/b}{\sqrt{1 + (a/b)^2}}\right] - (1 - \cos\theta) \tag{6}$$

$$f = \frac{\rho_o}{\rho_s}\left[\frac{2 + (\Delta_o/r)}{1 + (\Delta_o/r)} - \left(\frac{\rho_1}{\rho_o} - 1\right)\frac{\Delta_o}{R}\right] \tag{7}$$

In cases where the cone is not infinitely slender, the tangential flow component must also be taken into account. Experimental evidence obtained for the present study indicates that the shock envelope is conical up to high angles of attack. With the shape of the shock thus defined, it is possible to derive expressions on the basis of flow continuity and the geometric properties of the body to determine the shock standoff angle β as well as the shock radius R indicated in figure 5. The details of this derivation are developed in appendix B and give the following:

$$\left.\begin{aligned} \beta &= \tan^{-1}\left[\left(\frac{\Delta}{b} + N\right)\tan\epsilon_y\right] \\ &\text{and} \\ R &= \frac{b}{\sqrt{1 + (a/b)^2}}\sin\theta \end{aligned}\right\} \tag{8}$$

where

$$\frac{\Delta}{b} = \frac{1 + \dfrac{\tan\epsilon_y}{\tan\alpha'}\left[\dfrac{\sin\theta}{6\sqrt{1 + (a/b)^2}} - \dfrac{4}{3}\dfrac{\rho_1'}{\rho_o}N\right]}{\sqrt{1 + \left(\dfrac{a}{b}\right)^2}\left(\dfrac{\sin\theta}{\Delta/R}\right) + \dfrac{\tan\epsilon_y}{\tan\alpha'}\left(2 - \dfrac{\rho^*}{\rho_1'}\right)\dfrac{\rho_1'}{\rho_o}}$$

$$N = \frac{\left\{\dfrac{1 - \cos\theta}{\sin\theta} + \dfrac{a}{b}\left[\dfrac{a}{b} - \sqrt{1 + \left(\dfrac{a}{b}\right)^2}\right]\right\}}{\sqrt{1 + \left(\dfrac{a}{b}\right)^2}}$$

and

$$\alpha' = \beta + \alpha + \epsilon_z$$

Values of f used were the same as those for the capsule. The basis for this is explained in appendix B. Values for θ and Δ/R are given in the charts of figure 6 as a function of density ratio ρ_1/ρ_o for various

parameters a/b. The same assumptions were made in regard to gas properties as in the charts of figure 4. In the application of θ and Δ/R in equation (8), however, the density ratio is ρ_1'/ρ_o, that of an oblique shock at angle α'. Since α' is a function of β, the angle in question, iterative calculations beginning with an initial assumption for the value of β are required. However, trial computations quickly converge to the solution. The validity of the solution is restricted at high angles of attack to the angle range wherein the sum of the thickness angle ϵ_z, the shock angle β, and the angle of attack α is less than approximately 90°. When the sum of these angles is greater than 90°, the tangential flow component is reversed and the flow can no longer be conical. The validity is restricted at low angles of attack; if $M_o \sin \alpha'$ is less than about 2, the components of mass flow are not given accurately in the present simplified treatment.

COMPARISONS OF ANALYTICAL AND EXPERIMENTAL RESULTS

This section of the report will first establish the validity of the results of the present method in determining shock standoff distance for simple symmetrical shapes at zero angle of attack by comparison with the results of the more accurate methods of Van Dyke and Belotserkovski and with those of experiment. Next, the results of the method in determining shock shapes of capsule- and conical-type vehicles at angles of attack will be compared with experimental measurements.

Figures 7 and 8 show a comparison of analytical results for symmetrical shapes at zero angle of attack with available experimental results. Agreement between the results of the present analysis with those of Van Dyke and Belotserkovski and with experimental values is satisfactory.

Figure 9 gives examples of experimental and estimated shock envelope traces about capsule-type vehicles for several angles of attack and Mach numbers. Only one example is presented wherein appreciable real-gas effects were involved. This is the capsule at Mach number 14.9 which was tested at a simulated altitude of 30,000 feet at a velocity of 10,180 feet per second. Generally, the experimental and estimated shock envelopes are in good agreement.

In figure 10 calculated and experimental results for the shock angle of a family of elliptic cones are shown as a function of angle of attack. The cones have thickness-to-span ratios of 0 (a flat plate), 1/3, and 1 (a circular cone). The results are for a Mach number of 4. The limiting lines shown indicate the angle-of-attack range for which the analysis is applicable. Agreement between predicted and experimental results is good.

In figure 11 predicted and experimental shock standoff angles are compared for blunted as well as sharp-nosed conical shapes. The nose of a blunted conical shape is treated as a capsule-type vehicle and the shock angle for the conical part of the shock envelope is faired to the capsule solution at the point of equal slope. The data of figure 11 are for angles of attack from 20° to 70° and for Mach numbers from 3 to 10. Good agreement between experimental and theoretical results is noted.

CONCLUDING REMARKS

Simple methods were developed for predicting shock envelopes about two types of atmosphere entry vehicles at angle of attack. Predicted shock envelope shapes for capsule-type vehicles were compared with experimental values for air flows within the Mach number range 3 to 14.9 and the angle-of-attack range up to 33°. Predicted shock standoff angles for conical vehicles were compared with experimental values for air flows within the Mach number range 3 to 10 and the angle-of-attack range 20° to 70°.

The methods are applicable to perfect-gas flows and to equilibrium flows of real gases. Charts were developed specifically for predicting shock envelopes.

Satisfactory agreement between predicted and experimental shock envelopes was found for the range of flow conditions covered by the comparisons. Except for one case, only perfect-air conditions were covered, thus essentially limiting the evaluation of the methods of prediction to the perfect-air case. For the evaluation of the methods for high-enthalpy, equilibrium flow of real gases, further experimental research is needed.

Ames Research Center
National Aeronautics and Space Administration
Moffett Field, Calif., Mar. 6, 1961

APPENDIX A

NOTATION

a	vertical axis of elliptic cone, ft
b	horizontal axis of elliptic cone, ft
b'	spanwise distance to sonic point on elliptic cone, ft
f	shock correlation function
M	Mach number
m	mass-flow component
R	shock radius, ft
r	stagnation point body radius, ft
V	stream velocity, ft/sec
X,Y,Z	Cartesian coordinates
Δ	shock standoff distance from sonic point on body, ft
Δ_o	shock standoff distance from stagnation point on body, ft
α	angle of attack, deg
α'	conical shock angle with respect to free-stream direction in vertical plane of symmetry, deg
β	angle between conical shock and body in vertical plane of symmetry, deg
δ	flow deflection angle through oblique shock, deg
ϵ	half-angle subtended by capsule forebody arc, deg
ϵ_y	cone semiapex angle in plane of horizontal axis, deg
ϵ_z	cone semiapex angle in plane of vertical axis, deg
θ	inclination of shock element opposite sonic point on body with respect to free stream or to crossflow stream (see fig. 2), deg

γ specific-heat ratio

ρ density, lb/ft^3

ρ_1 density behind normal shock, lb/ft^3

ρ_1' density behind shock inclined at angle α', lb/ft^3

φ inclination of body surface at sonic point with respect to plane normal to free-stream direction, deg

Subscripts

o free-stream conditions

s stagnation point on body

θ point behind shock element at θ degrees

$*$ sonic point on body

APPENDIX B

DERIVATION OF EQUATIONS

The following sections give the details of the derivation of the equations defining the shock envelopes for capsule- and conical-type vehicles. Numerical examples are also presented.

CAPSULE-TYPE VEHICLES

Flow Continuity Equations

Mass-flow continuity is satisfied for an elemental volume between the shock and the body as shown in figure 12. The flow is three-dimensional and assumed to proceed radially from the stagnation streamline. Mass flow passes out from the volume through a strip of unit width and length Δ. The arithmetic mean of the vertical components of mass flow at the sonic point on the body and at the shock-wave position, θ, opposite the sonic point is utilized. The component at the sonic point is equal to the product of cosine φ and the mass flow passing through a normal shock and expanding isentropically to sonic value. This product, expressed as a mass flow per unit area and normalized with respect to the free-stream value $\rho_o V_o$, is

$$\frac{\rho_* V_*}{\rho_o V_o} \cos \varphi = \sqrt{\frac{\rho_1}{\rho_o}} \left[\frac{2}{\left(1 + \frac{\rho_o}{\rho_1}\right) + \gamma \left(1 - \frac{\rho_o}{\rho_1}\right)} \right]^{\frac{1}{\gamma - 1}} \cos \varphi \tag{B1}$$

The component of mass flow per unit area at the shock normalized with respect to the free-stream value is given by oblique-shock relationships as

$$\frac{1}{2} \left(\frac{\rho_\theta}{\rho_o} - 1 \right) \sin 2\theta \tag{B2}$$

The mass flow passing out of the volume element is then

$$\frac{\Delta}{2} \left[\frac{\rho_o V_o}{2} \left(\frac{\rho_\theta}{\rho_o} - 1 \right) \sin 2\theta + \rho_* V_* \cos \varphi \right] \tag{B3}$$

Similarly, the product of entering unit-area mass flow $\rho_o V_o$ and the projected "wedge" strip area $(1/2)R \sin \theta$ gives

$$\frac{\rho_o V_o}{2} R \sin \theta \tag{B4}$$

Expressions (B3) and (B4) are equated and rearranged to give equation (1).

$$\frac{\Delta}{R} = \frac{\sin \theta}{\frac{1}{2}\left(\frac{\rho_\theta}{\rho_o} - 1\right) \sin 2\theta + \frac{\rho_* V_*}{\rho_o V_o} \cos \varphi} \tag{1}$$

Geometric Relationships

A necessary step in subsequent shock solutions is to relate the shock standoff distance, Δ, at the sonic point to the standoff distance, Δ_o, at the stagnation point. Since the capsule forebody and the shock elements are circular, these standoff distances are related as follows:

$$\Delta = \Delta_o + r(1 - \cos \varphi) - R(1 - \cos \theta) \tag{B5}$$

The above equation normalized with respect to shock radius R gives equation (2).

$$\frac{\Delta}{R} = \frac{\Delta_o}{R} + \frac{r}{R}(1 - \cos \varphi) - (1 - \cos \theta) \tag{2}$$

Velocity Gradient Correlation

It has been shown in reference 1 that the stagnation-point velocity gradient in the dimensionless form $\frac{\Delta_o}{V_o} \frac{dV/ds}{(1 + \Delta_o/r)}$ is a function of Mach number (or normal-shock density ratio) and correlates data involving a wide variety of axisymmetric shapes. In the following derivation the above stagnation-point velocity gradient will be equated to a more convenient correlation function in which the velocity terms are eliminated and in which only shock standoff distance, body radius, and shock radius terms appear.

Continuity of mass flow is considered for a small conical volume element centered on the stagnation streamline as shown in figure 13. The line 0-1 represents an element of the volume extending from the shock to

the body. The flow is deflected $(\delta + d\varphi)$ with respect to 0-1 at point 0 on the shock. Oblique shock relationships for small θ give $\delta = (\rho_1/\rho_o - 1)d\theta$. Geometrical considerations give $(\Delta_o + r)d\varphi = R\, d\theta$, so that $\delta + d\varphi = \left[\left(\frac{\rho_1}{\rho_o} - 1\right)\frac{\Delta_o + r}{R} + 1\right]d\varphi$. The unit-area mass flow at 0 normal to 0-1 is then $\rho_o V_o\left[\left(\frac{\rho_1}{\rho_o} - 1\right)\frac{\Delta_o + r}{R} + 1\right]d\varphi$. The unit-area mass flow at 1 is $[d(\rho V)/ds]r\, d\varphi$, a value to be determined. The arithmetic mean of the mass flow leaving the conical surface of length Δ_o is equated to that entering the projected surface of radius $(r + \Delta_o)d\varphi$. The resulting equation is

$$\frac{\Delta_o}{2}\left\{2\pi(r + \Delta_o)d\varphi(\rho_o V_o)\left[\left(\frac{\rho_1}{\rho_o} - 1\right)\left(\frac{\Delta_o + r}{R}\right) + 1\right]d\varphi + 2\pi r\, d\varphi\left[\frac{d(\rho V)}{ds}\right]r\, d\varphi\right\}$$
$$= \rho_o V_o \pi(r + \Delta_o)^2 d\varphi^2$$

The stagnation-point mass-flow gradient $d(\rho V)/ds$ given by the above identity is

$$\frac{d(\rho V)}{ds} = \frac{\rho_o V_o}{\Delta_o}\left(1 + \frac{\Delta_o}{r}\right)\left[1 - \left(1 + \frac{\Delta_o}{r}\right)\left(\frac{\rho_1}{\rho_o} - 1\right)\frac{\Delta_o}{R}\right] \tag{B6}$$

At the stagnation point $V = 0$, $\rho = \rho_s$, $d\rho/ds = 0$, so $d(\rho V) = \rho_s dV$. Equation (B6) is rearranged to give

$$\frac{\Delta_o \frac{dV}{ds}}{V_o\left(1 + \frac{\Delta_o}{r}\right)} = \frac{\rho_o}{\rho_s}\left[1 - \left(1 + \frac{\Delta_o}{r}\right)\left(\frac{\rho_1}{\rho_o} - 1\right)\frac{\Delta_o}{R}\right] \tag{B7}$$

where

$$\frac{\rho_o}{\rho_s} = \frac{\rho_o}{\rho_1}\left(1 - \frac{\gamma - 1}{\gamma + 1}\frac{\rho_o}{\rho_1}\right)^{\frac{1}{\gamma - 1}}$$

It is convenient, for reasons to be discussed later, to apply the factor 2 to equation (B7), thus

$$\frac{2\Delta_o \frac{dV}{ds}}{V_o\left(1 + \frac{\Delta_o}{r}\right)} = 2\frac{\rho_o}{\rho_s}\left[1 - \left(1 + \frac{\Delta_o}{r}\right)\left(\frac{\rho_1}{\rho_o} - 1\right)\frac{\Delta_o}{R}\right]$$

or, letting f replace the left-hand term,

$$f = 2\,\frac{\rho_o}{\rho_s}\left[1 - \left(1 + \frac{\Delta_o}{r}\right)\left(\frac{\rho_1}{\rho_o} - 1\right)\frac{\Delta_o}{R}\right] \tag{3}$$

Numerical Example

The charts of figure 4 are now applied to an example calculation of the shock trace about the lenticular forebody shown in figure 2. The forebody arc subtends a half-angle ϵ of 30°. The flight condition is $M = 6.3$, $\rho_1/\rho_o = 5.33$, at angle of attack of 16°. At this angle the upper sonic point (1) is at the corner and is inclined $\varphi_1 = (30^\circ - 16^\circ) = 14^\circ$. The lower sonic point (2) is on the body where $\varphi_2 = 45^\circ$. The relative locations of the sonic points are $(X_2 - X_1) = 4.30$ and $|Y_1| + |Y_2| = 15.60$. The values $\Delta/R_1 = 0.106$, $\theta_1 = 16.5^\circ$, $\Delta/R_2 = 0.175$, and $\theta_2 = 31.4^\circ$ are found in figure 5. Equations (4) are numerically evaluated as follows:

$$X_1 = \frac{15.60 - 4.30\left(\dfrac{0.521}{0.175 + 0.147}\right)}{\left(\dfrac{0.284}{0.106 + 0.041}\right) + \left(\dfrac{0.521}{0.175 + 0.147}\right)} = 2.43$$

$$Y_1 = \frac{2.43 \times 0.284}{0.106 + 0.041} = 4.71$$

$$Y_2 = 15.60 - 4.71 = 10.89$$

$$R_1 = \frac{4.71}{0.284} = 16.56$$

$$R_2 = \frac{10.89}{0.521} = 20.9$$

CONICAL VEHICLES

Flow Continuity and Geometric Considerations

Detailed derivations of equations defining the shock envelope about conical vehicles are developed with the aid of figure 14. In this figure are shown three views of a section of an elliptic cone at angle of attack α. The flow is assumed to be conical. The shock element in the vertical plane of symmetry inclined at angle α' is taken to be along the X axis. A volume element of length dx between the shock and the body surface is bounded by the vertical plane of symmetry poo'p' and the surface containing sonic line nn' and its projection onto the shock surface, mm'. Continuity of mass flow is satisfied for this volume element.

To write the continuity equation it is necessary to evaluate projected areas of the various surfaces of the volume element. Area mnop is similar to area m'n'o'p' since the shock envelope and body surface are conical with respect to a common origin. Thus

$$\left.\begin{aligned} \frac{S_{mnop}}{l^2} &= \frac{S_{m'n'o'p'}}{(l + dx)^2} \\ \text{or} \qquad & \\ S_{m'n'o'p'} &= S_{mnop}\left(1 + \frac{2dx}{l}\right) \end{aligned}\right\} \qquad \text{(B8)}$$

where

$$S_{mnop} = \frac{b'}{3}(2\Delta_o + \Delta)$$

It should be noted that the control surface intercepting the tangential mass-flow component is not normal to the axis of the body. Therefore, in the plane of the control surface, the ellipticity of the associated body section is different from the true cross-sectional value. The relative distortion in ellipticity is of the order $\cos(\epsilon_Z - \beta)$. Since ϵ_Z and β are usually small and in any event tend to cancel, the error resulting from section distortion is neglected. The distance from the sonic point (where surface slope of 45° is assumed) to the vertical plane of symmetry is

$$R \sin \theta = b' = \frac{b}{\sqrt{1 + \left(\frac{a}{b}\right)^2}} \qquad \text{(B9)}$$

The relationship between sonic-point (Δ) and center line (Δ_o) shock standoff distance in terms of semispan b is then

$$\frac{\Delta}{b} = \frac{\Delta_o}{b} - \frac{\dfrac{1 - \cos\theta}{\sin\theta} + \dfrac{a}{b}\left[\dfrac{a}{b} - \sqrt{1 + \left(\dfrac{a}{b}\right)^2}\right]}{\sqrt{1 + \left(\dfrac{a}{b}\right)^2}} = \frac{\Delta_o}{b} - N \tag{B10}$$

Equations (B8) to (B10) and the terms indicated on figure 14, are used to project the following areas on the Y-Z plane,

$$S_{mnop} = \frac{b(3\Delta + 2Nb)}{3\sqrt{1 + \left(\dfrac{a}{b}\right)^2}}$$

$$S_{m'mpp'} = \frac{R(1 - \cos\theta)b'dx}{3l} \quad \frac{b^2(\sin\theta)dx}{6\left[1 + \left(\dfrac{a}{b}\right)^2\right]l}$$

$$S_{m'n'nm} = \frac{\Delta b\ dx}{\sqrt{1 + \left(\dfrac{a}{b}\right)^2}\ l}$$

on the X-Y plane,

$$S_{nm'p'p} = b'dx = \frac{b\ dx}{\sqrt{1 + \left(\dfrac{a}{b}\right)^2}}$$

and on the X-Z plane,

$$S_{mnn'm'} = \Delta\ dx$$

Next, the values of the mass-flow components per unit area (ρV) normal to each area are required. All velocities in the X direction are taken as $V_o \cos\alpha'$, being substantially tangent to the shock. The density within the control volume varies from a maximum of $\rho_s' > \rho_1'$ at line oo' to a minimum of $\rho^* < \rho_1'$ at the sonic line nn'. The density distribution is approximately accounted for by assuming ρ' as the mean density of the flow through the surfaces mnop and m'n'o'p', and

ρ^* as the mean density through the surface $m'n'nm$. The sonic value $\rho^* = \rho_1'[2/(\gamma + 1) - (\gamma - 1)(\rho_o/\rho_1')]^{1/(\gamma-1)}$ is used. The unit-area mass flow (m) in the Y direction through $mnn'm'$ is $\rho_o V_o[\sin\theta/(\Delta/R)]$. Values for θ and Δ/R are determined from figure 7 with ρ_1'/ρ_o in place of ρ_1/ρ_o. Summation of all unit mass-flow products with their associated areas is then made to satisfy the continuity of flow. Omitting the detailed algebraic steps involved yields the following equation:

$$\frac{\Delta}{b} = \frac{1 + \dfrac{\tan\epsilon_y}{\tan\alpha'}\left[\dfrac{\sin\theta}{6\sqrt{1 + (a/b)^2}} - \dfrac{4}{3}\dfrac{\rho_1'}{\rho_o}N\right]}{\sqrt{1 + \left(\dfrac{a}{b}\right)^2}\left(\dfrac{\sin\theta}{\Delta/R}\right) + \dfrac{\tan\epsilon_y}{\tan\alpha'}\left(2 - \dfrac{\rho^*}{\rho_1'}\right)\dfrac{\rho_1'}{\rho_o}} \tag{B11}$$

Equation (B11) along with the following geometric relationships permits calculation of the shock angle β as a function of angle of attack α.

$$\beta = \tan^{-1}\left[\left(\frac{\Delta}{b} + N\right)\tan\epsilon_y\right] \tag{8}$$

$$N = \frac{\left\{\dfrac{1 - \cos\theta}{\sin\theta} + \dfrac{a}{b}\left[\dfrac{a}{b} - \sqrt{1 + \left(\dfrac{a}{b}\right)^2}\right]\right\}}{\sqrt{1 + \left(\dfrac{a}{b}\right)^2}}$$

and

$$\alpha' = \beta + \alpha + \epsilon_z$$

Velocity Gradient Correlation

Equation (7) is derived on the basis of two-dimensional flow through a differential volume element in the vicinity of the stagnation streamline in a manner similar to that in the case of axisymmetric flow. Values for f given by equation (7), plotted in figure 3, were obtained by using the theoretical stagnation-point standoff distance and shock radii given in reference 3 for circular cylinders. Under conditions of the same ratio for Δ_o/V_o the stagnation-point velocity gradient for axisymmetric flow can be shown to be one-half the value for two-dimensional flow due

to radial "relief." Accordingly, the factor 2 applied to the axisymmetric velocity gradient places it in correlation with two-dimensional gradients, thus relating both two- and three-dimensional shock distance parameters to the same function f of density ratio.

The derivation of two-dimensional stagnation-point velocity gradients proceeds as follows: The line 0-1 in figure 13 in two-dimensional flow represents the side surfaces of a wedge of unit depth. The mass flows per unit area at 0 and at 1 remain the same as in the axisymmetric case. They are, respectively,

$$\rho_o V_o\left[\left(\frac{\rho_1}{\rho_o} - 1\right)\left(\frac{\Delta_o + r}{R}\right) + 1\right]d\varphi$$

and

$$\frac{d(\rho V)}{ds}\, r\, d\varphi$$

The product of the entering mass-flow per unit area with the area of surface 0-0 is $\rho_o V_o 2(r + \Delta_o)d\varphi$. This is equated to the product of the mean unit mass flow leaving surface 0-1 with the total area $2\Delta_o$.

$$2\Delta_o \frac{1}{2}\left\{\rho_o V_o\left[\left(\frac{\rho_1}{\rho_o} - 1\right)\left(\frac{\Delta_o + r}{R}\right) + 1\right] + \frac{d(\rho V)}{ds}\, r\right\} d\varphi = \rho_o V_o 2(r + \Delta_o)d\varphi$$

The stagnation-point mass-flow gradient $d(\rho V)/ds$ is given by reducing the above identity to

$$\frac{d(\rho V)}{ds} = \frac{\rho_o V_o}{\Delta_o}\left[\left(2 + \frac{\Delta_o}{r}\right) - \left(1 + \frac{\Delta_o}{r}\right)\left(\frac{\rho_1}{\rho_o} - 1\right)\frac{\Delta_o}{R}\right] \tag{B12}$$

At the stagnation point $V = 0$, $\rho = \rho_s$, $d\rho/ds = 0$, so $d(\rho V) = \rho_s dV$. Equation (B12) is arranged in the form

$$\frac{\Delta_o \frac{dV}{ds}}{V_o\left(1 + \frac{\Delta_o}{r}\right)} = \frac{\rho_o}{\rho_s}\left[\frac{2 + \frac{\Delta_o}{r}}{1 + \frac{\Delta_o}{r}} - \left(\frac{\rho_1}{\rho_o} - 1\right)\frac{\Delta_o}{R}\right]$$

or

$$f = \frac{\rho_o}{\rho_s}\left[\frac{2 + \frac{\Delta_o}{r}}{1 + \frac{\Delta_o}{r}} - \left(\frac{\rho_1}{\rho_o} - 1\right)\frac{\Delta_o}{R}\right] \tag{7}$$

It is to be remembered that r is the stagnation-point body radius; therefore, the application of equation (7) for elliptic bodies requires b^2/a in place of r.

Numerical Example

The shock angle β is calculated for an elliptic cone with $\epsilon_y = 15^\circ$, $\epsilon_z = 5^\circ$, and $a/b = 1/3$ at angle of attack $\alpha = 45^\circ$ at flight Mach number 6. An initial assumption that $\beta = 5^\circ$ is made; thus a trial value for $\alpha' = 5^\circ + 45^\circ + 5^\circ$ (see eqs. (8)). The crossflow Mach number is $6 \sin 55^\circ = 4.91$ at which $\rho_1'/\rho_o = 4.97$. Corresponding to this density ratio with $a/b = 1/3$, the charts of figure 6 give $\Delta/R = 0.234$ and $\theta = 13.6^\circ$. Equations (8) are then numerically evaluated as follows:

$$N = \frac{\left\{\frac{1 - 0.972}{0.237} + \frac{1}{3}\left[\frac{1}{3} - \sqrt{1 + \left(\frac{1}{3}\right)^2}\right]\right\}}{\sqrt{1 + \left(\frac{1}{3}\right)^2}} = -0.117$$

$$\frac{\Delta}{b} = \frac{1 + \frac{0.268}{1.427}\left[\frac{0.237}{6\sqrt{1 + (1/3)^2}} - \frac{4}{3}(4.97)(-0.117)\right]}{\sqrt{1 + \left(\frac{1}{3}\right)^2}\left(\frac{0.237}{0.234}\right) + \frac{0.268}{1.427}(2 - 0.693)4.97} = 0.504$$

$$\beta = \tan^{-1}[(0.484 - 0.117)0.268] = 5.9^\circ$$

The calculated value for β is sufficiently close to the assumed value that an iterated calculation is unnecessary.

The above example utilized the result for ρ_1'/ρ_o as given by oblique shock relationships for air with $\gamma = 1.4$. At higher velocities and at altitudes where large departures from ideal gas properties occur recourse must be taken to shock density versus velocity and altitude plots such as are given in reference 5. An initial value for ρ_1'/ρ_o is determined from such plots as that corresponding to the velocity $V_o \sin \alpha'$ at the altitude in question. Generally, one iteration is sufficient to fix α' and thus ρ_1'/ρ_o.

REFERENCES

1. Traugott, Stephen C.: An Approximate Solution of the Direct Supersonic Blunt-Body Problem for Arbitrary Axisymmetric Shapes. Jour. Aero. Sci., vol. 27, no. 5, May 1960, pp. 361-370.

2. Van Dyke, Milton D., and Gordon, Helen D.: Supersonic Flow Past a Family of Blunt Axisymmetric Bodies. NASA Rep. R-1, 1959.

3. Belotserkovsky, O. M.: Flow Past a Symmetrical Profile With a Detached Shock Wave. Jour. Appl. Math. and Mech., vol. 22, no. 2, March 1958, pp. 279-296.

4. Briggs, Benjamin R.: The Numerical Calculation of Flow Past Conical Bodies Supporting Elliptic Conical Shock Waves at Finite Angles of Incidence. NASA TN D-340, 1960.

5. Moeckel, W. E., and Weston, Kenneth C.: Composition and Thermodynamic Properties of Air in Chemical Equilibrium. NACA TN 4265, 1958.

6. Hochstim, Adolf R.: Gas Properties Behind Shocks at Hypersonic Velocities. I. Normal Shocks in Air. Convair Rep. No. ZPh(GP)-002, Jan. 30, 1957.

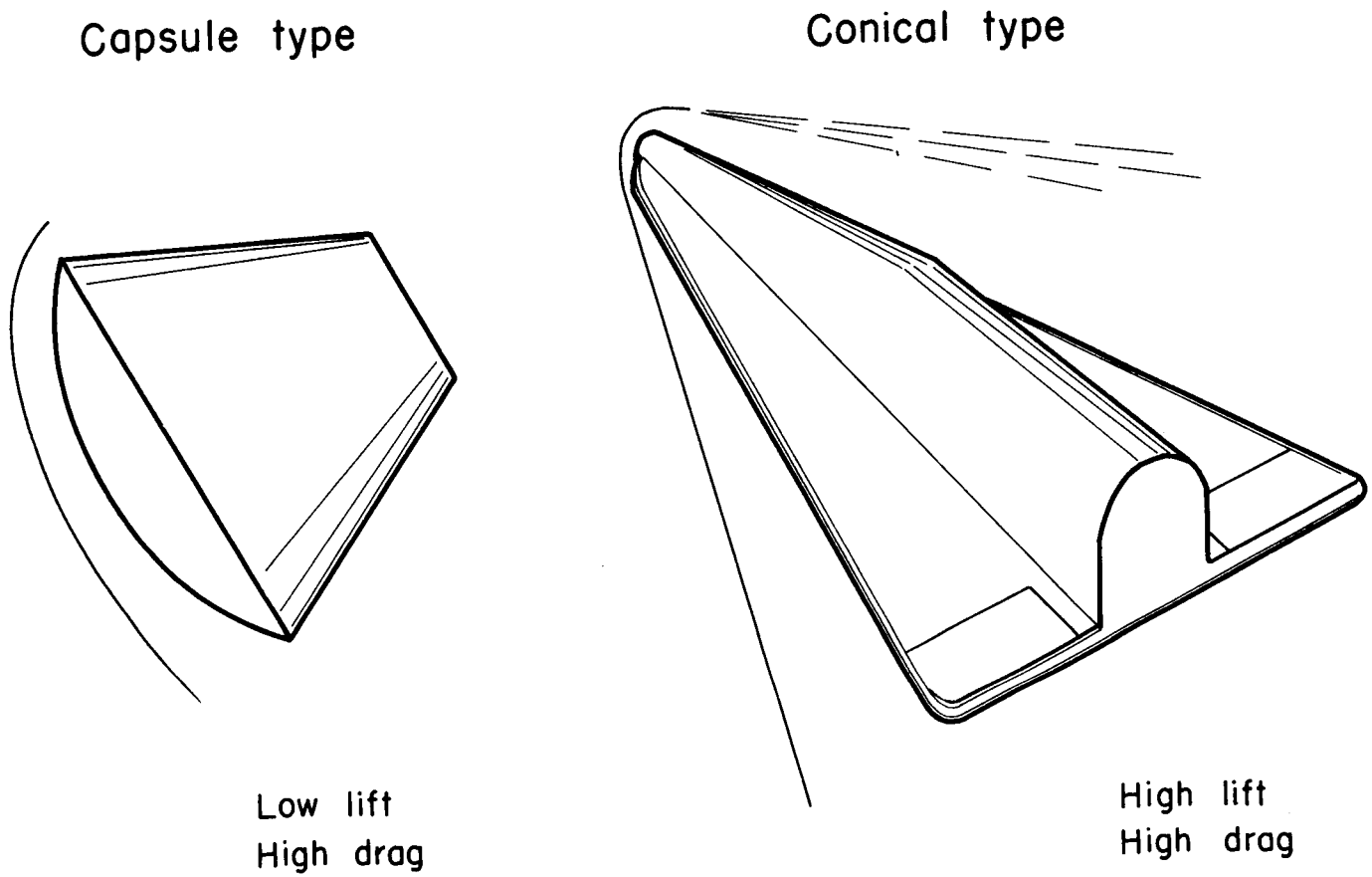

Figure 1.- Types of vehicles considered.

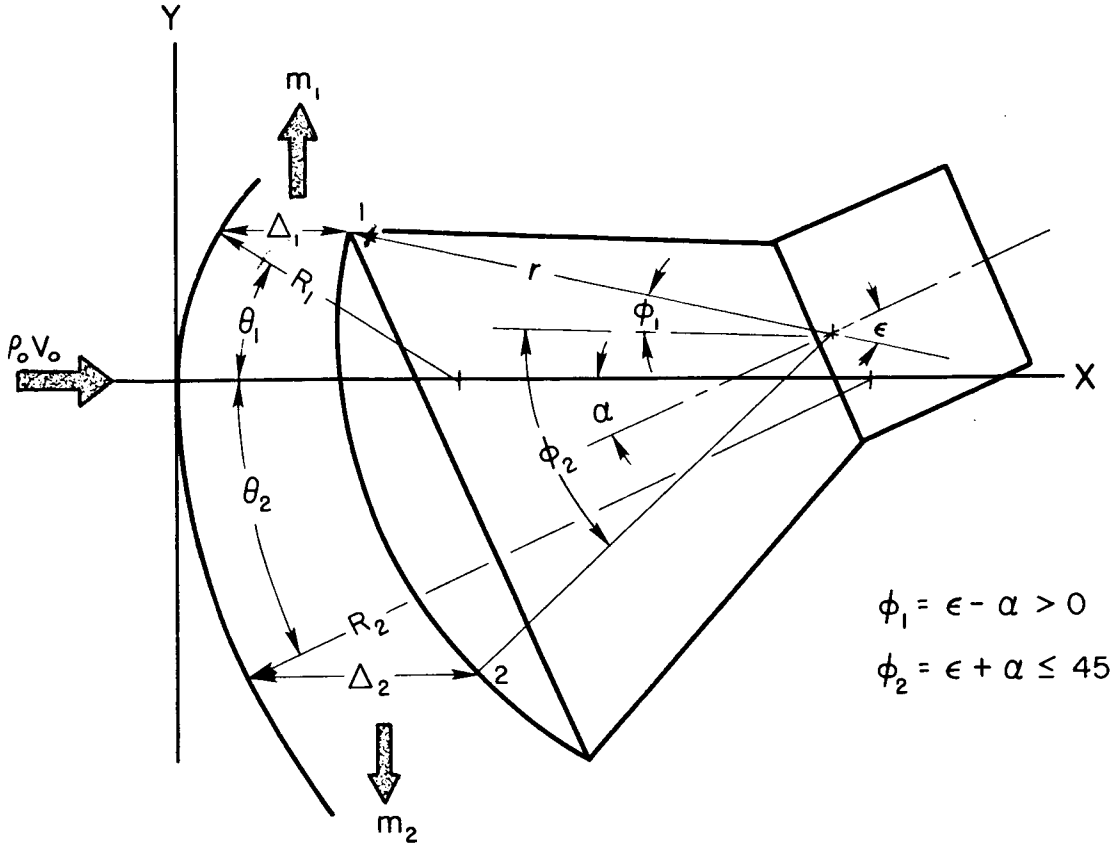

Figure 2.- Mass flow components for capsule-type vehicles.

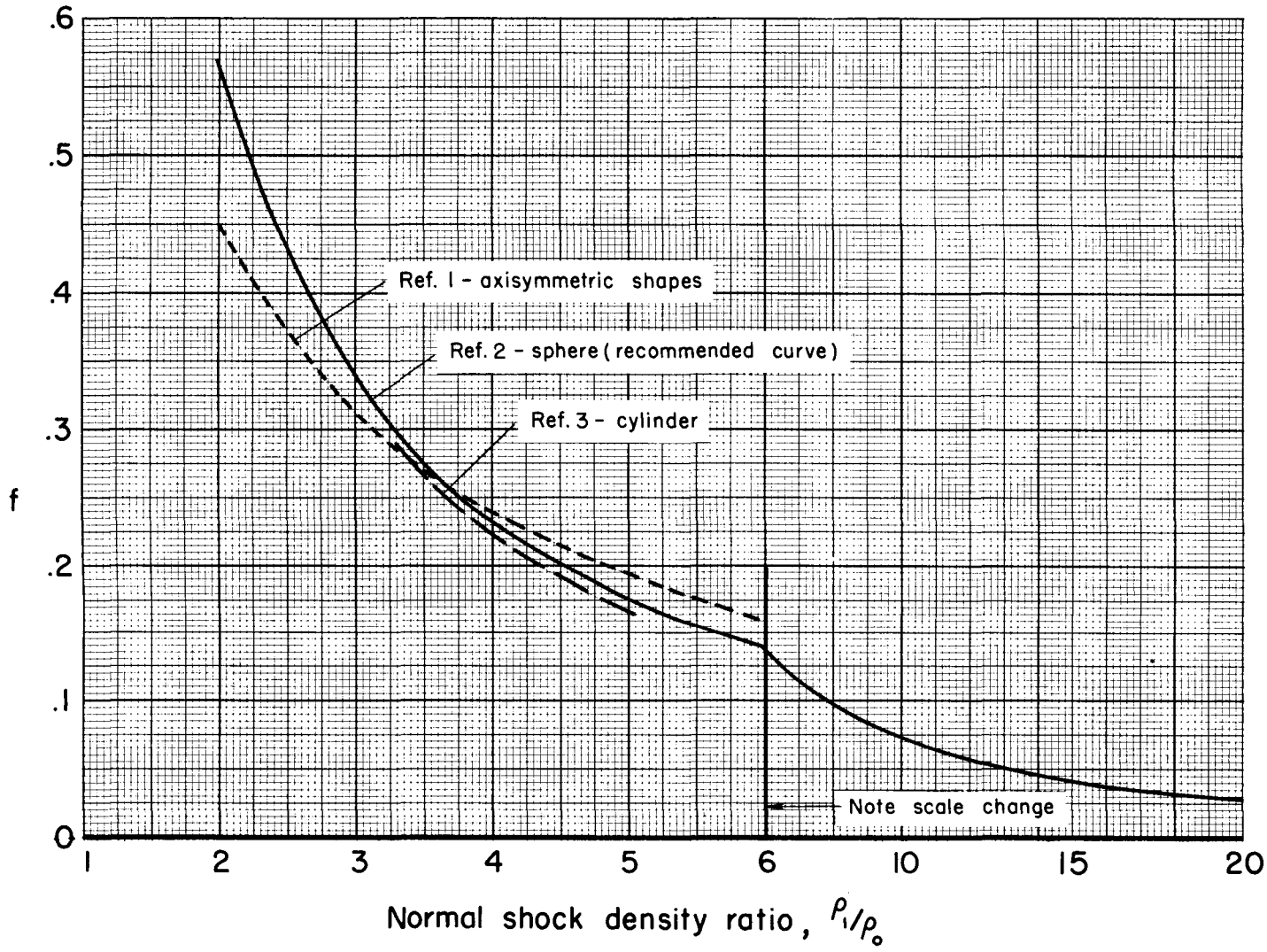

Figure 3.- Shock correlation function.

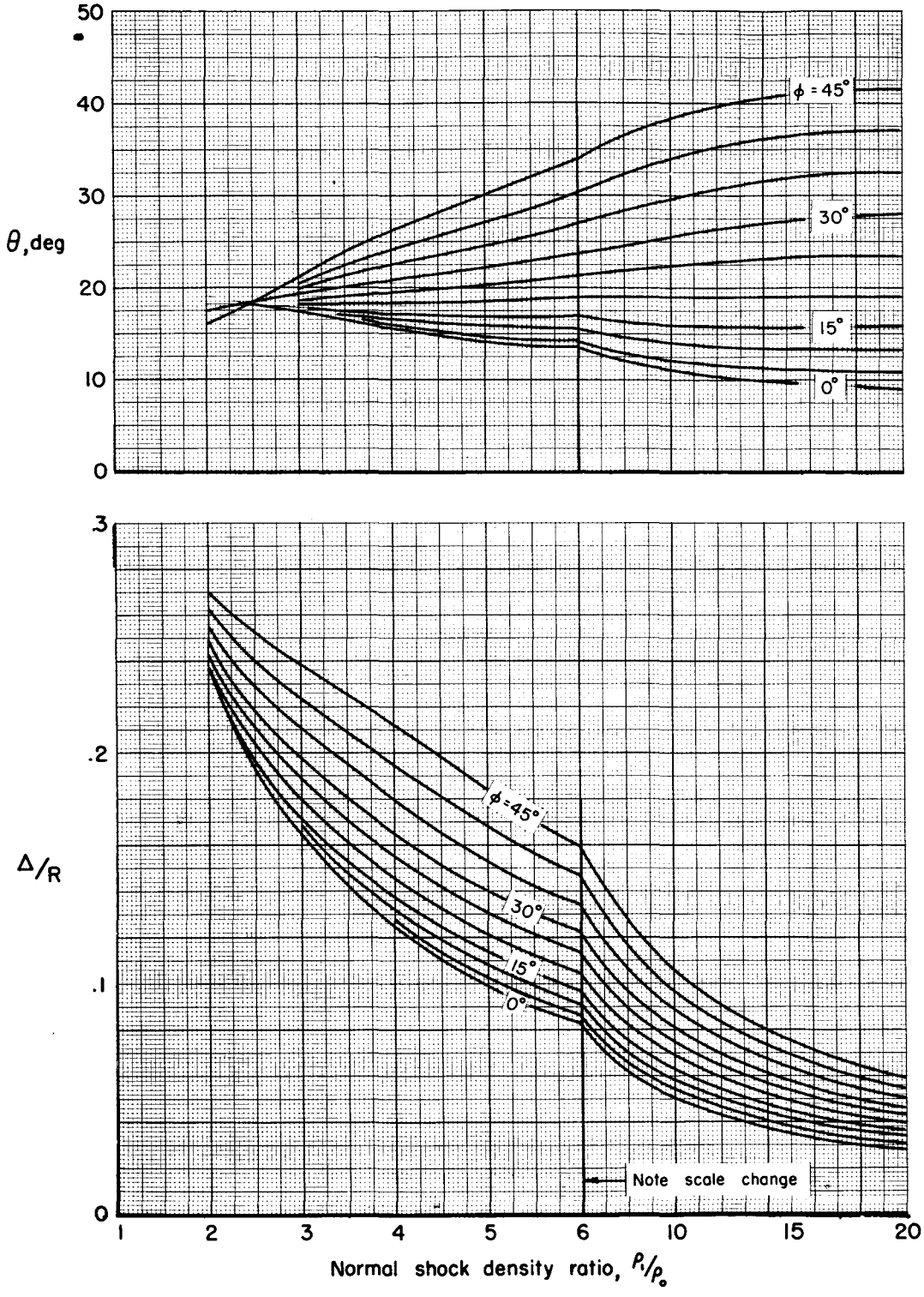

Figure 4.- Charts of Δ/R and θ for capsule-type vehicles.

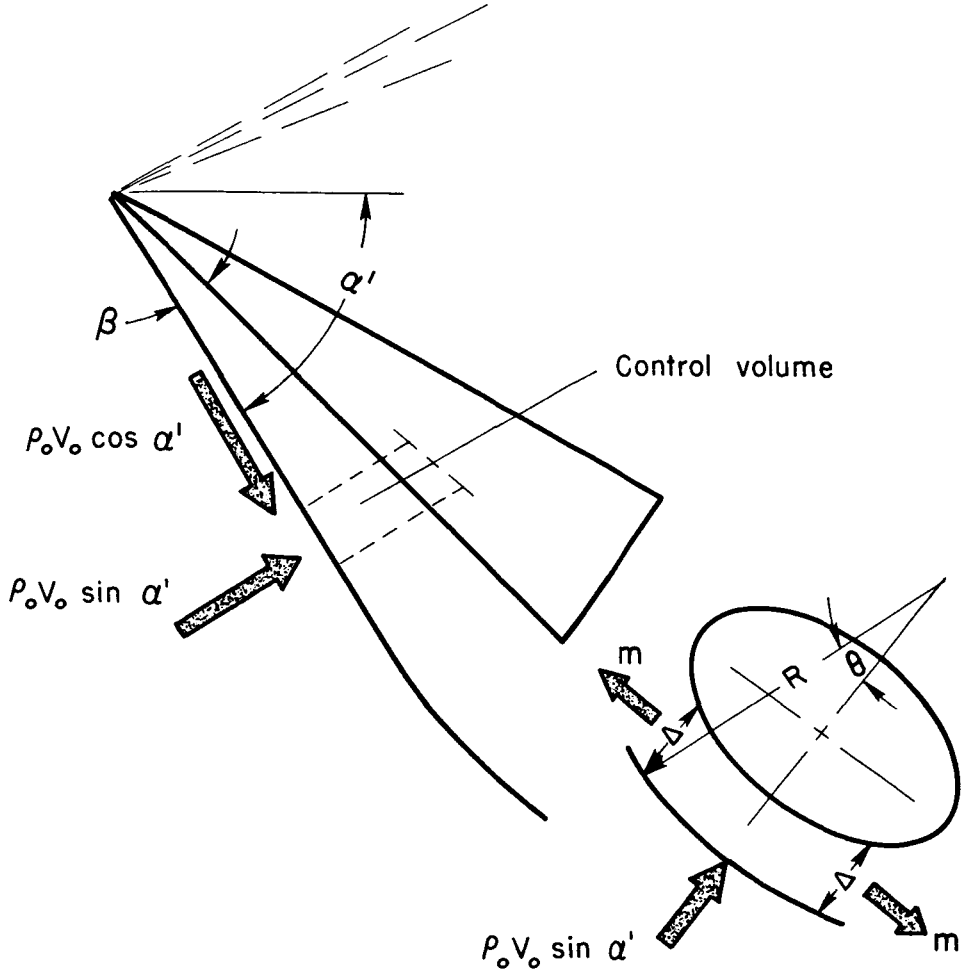

Figure 5.- Mass flow components for conical vehicles.

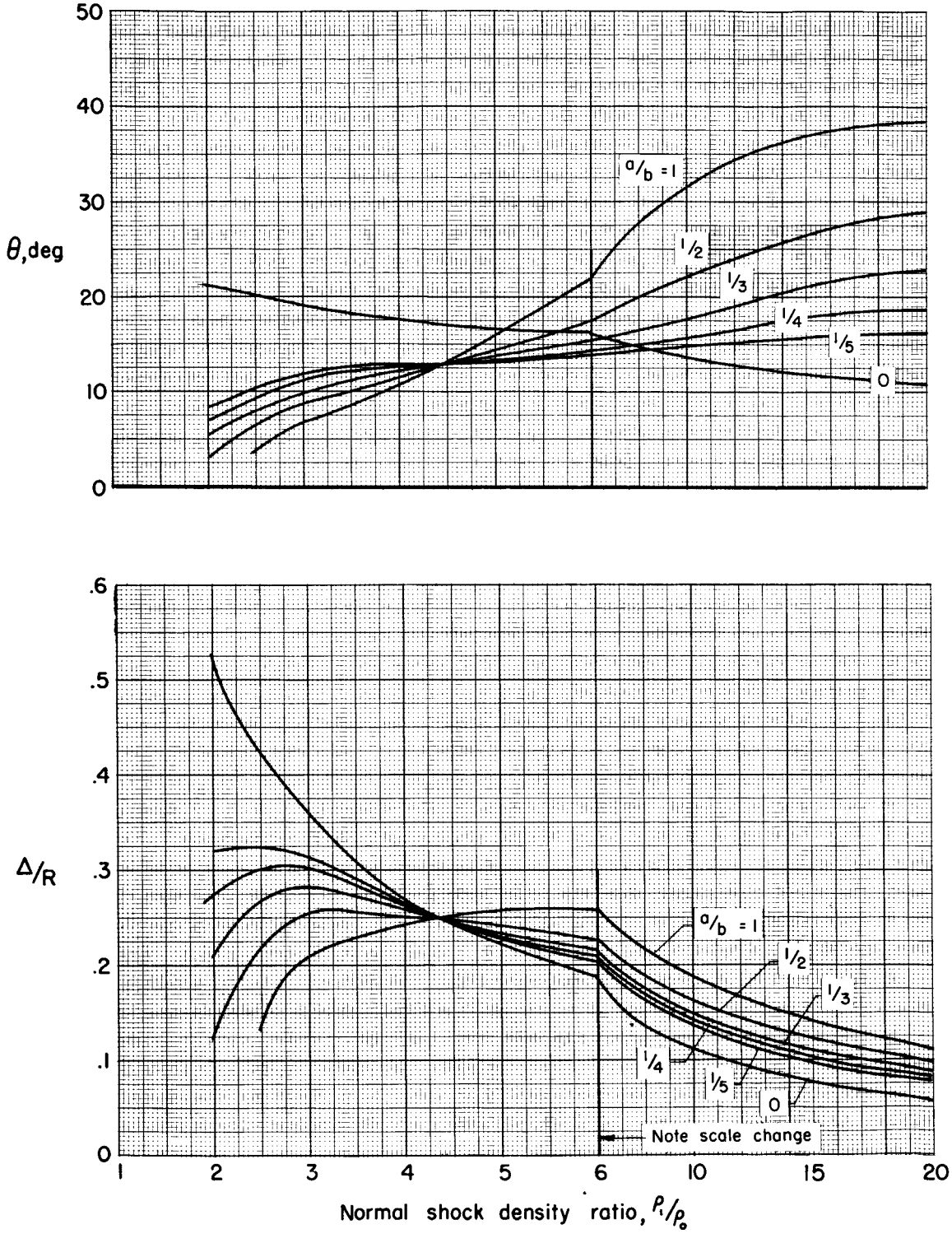

Figure 6.- Charts of Δ/R and θ for conical-type vehicles.

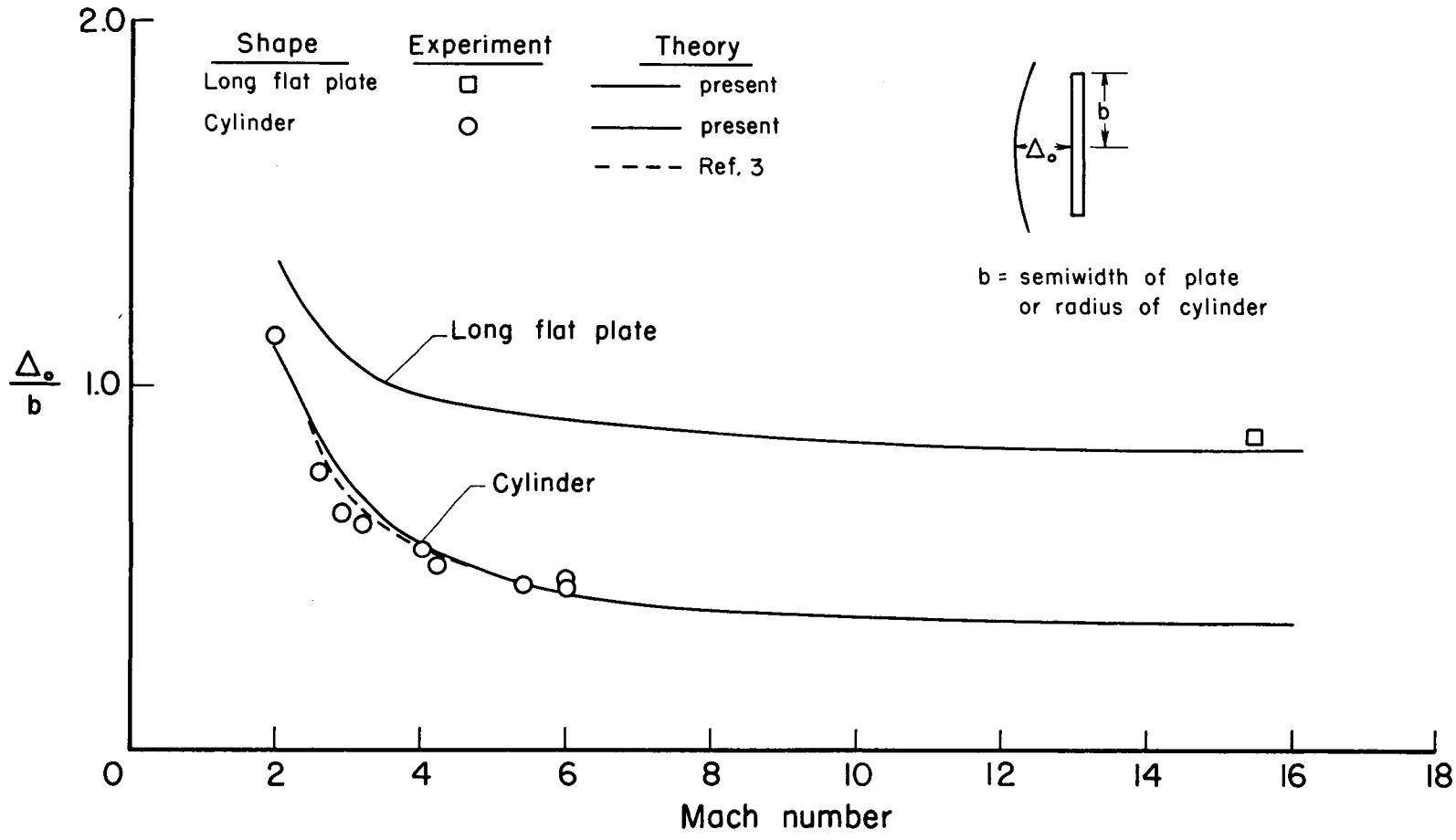

Figure 7.- Shock standoff distance for two-dimensional obstacles at zero angle of attack; air.

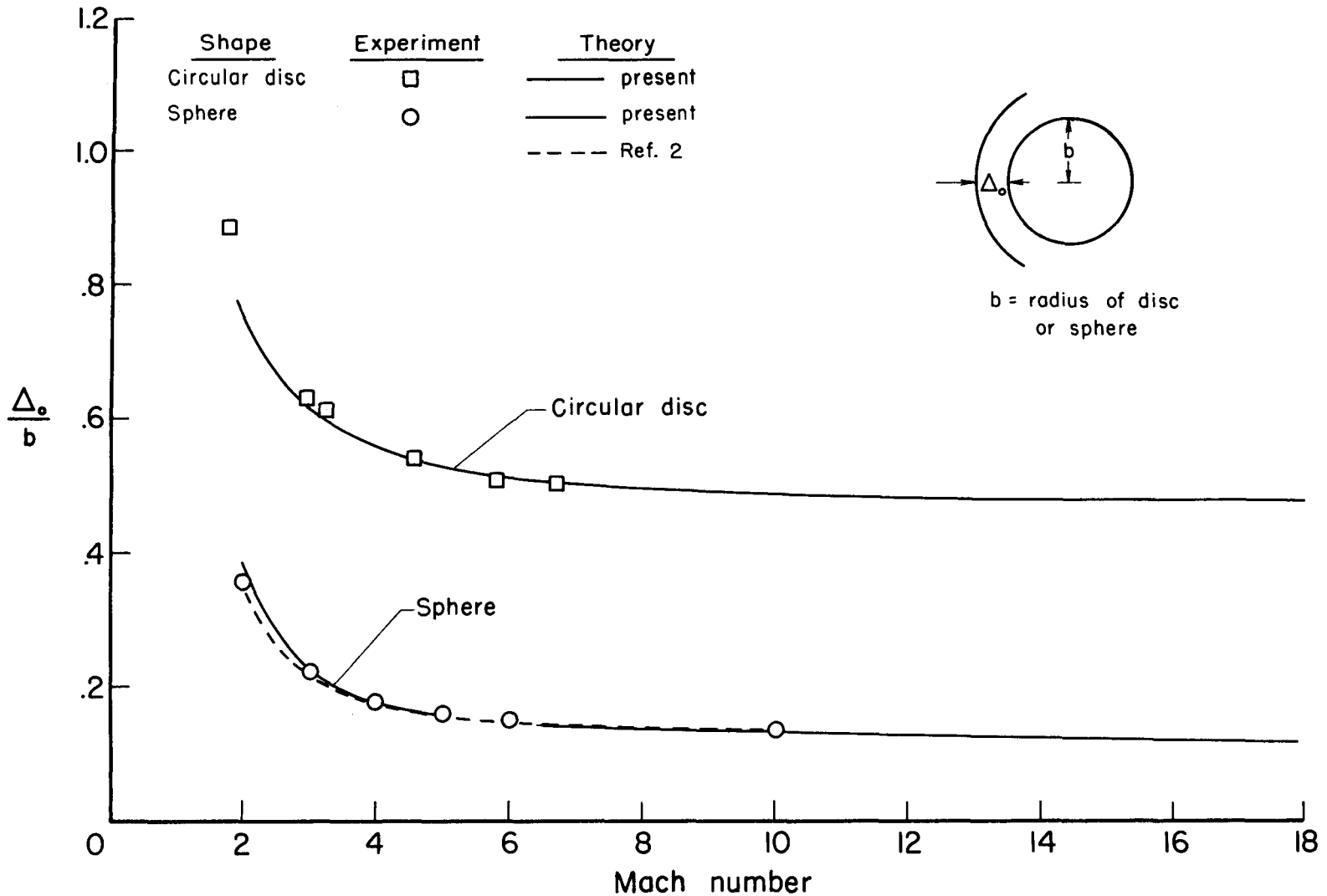

Figure 8.- Shock standoff distance for three-dimensional obstacles at zero angle of attack; air.

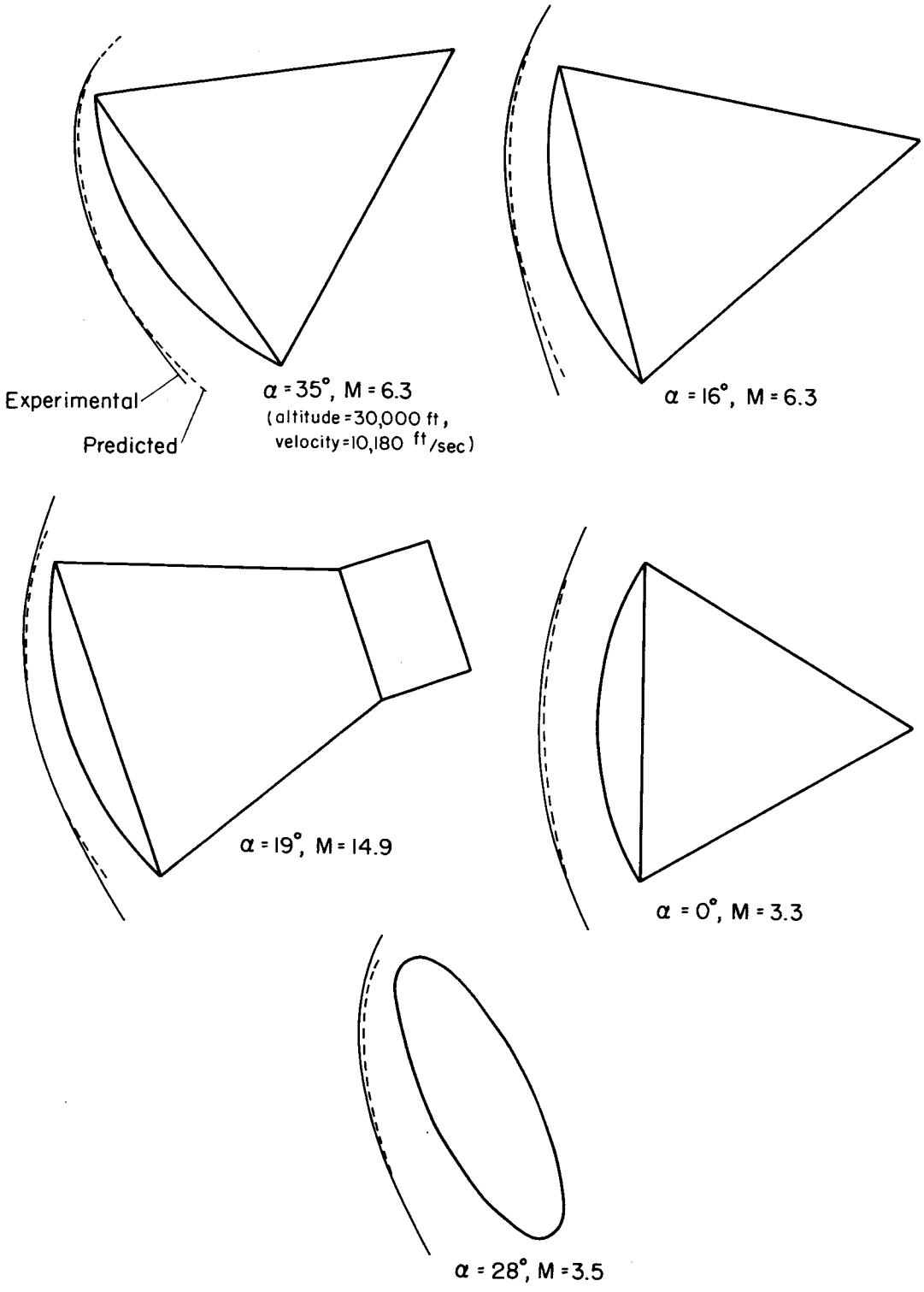

Figure 9.- Shock traces for capsule-type vehicles; air.

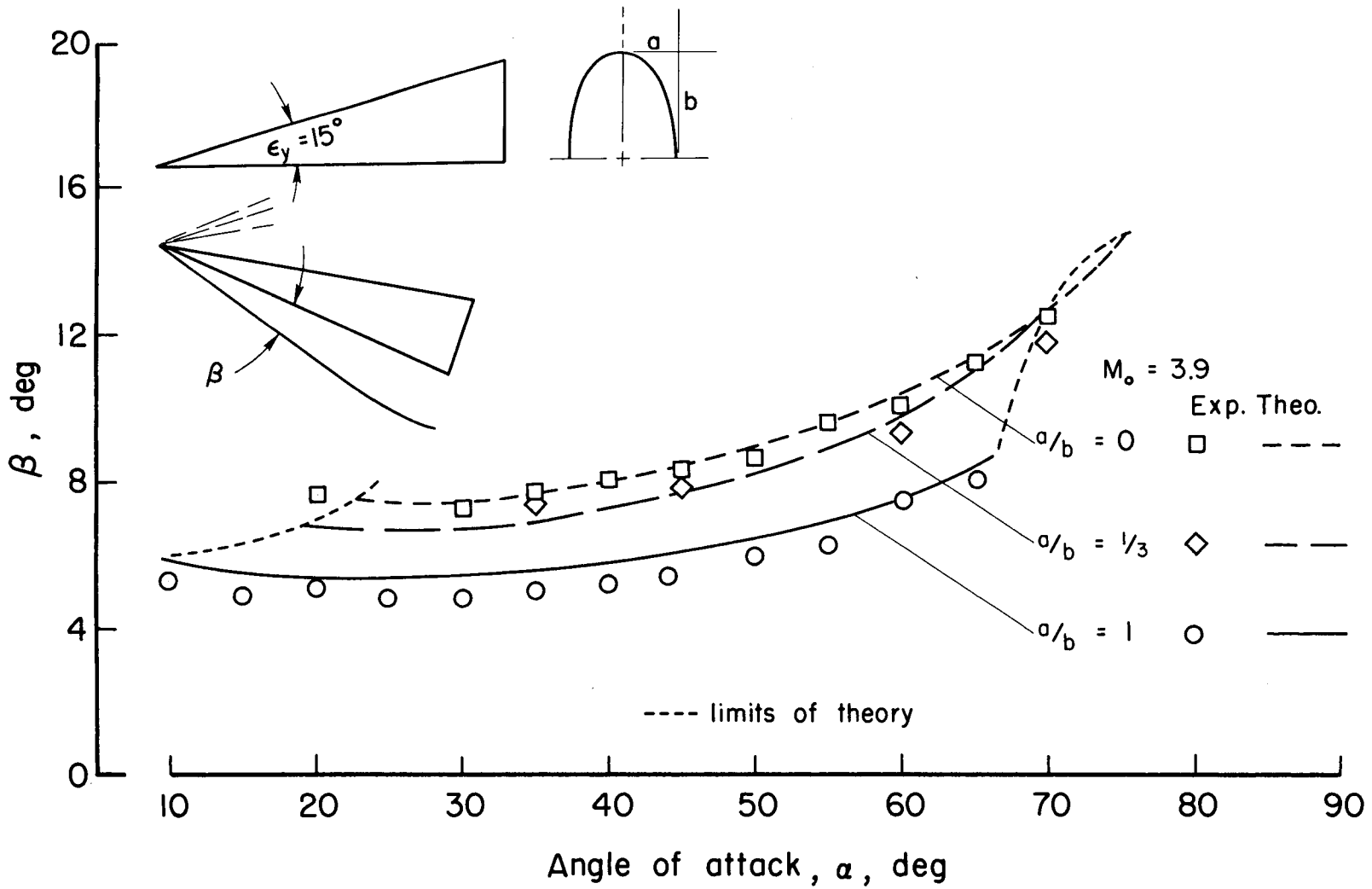

Figure 10.- Shock angles for a family of elliptic cones; air.

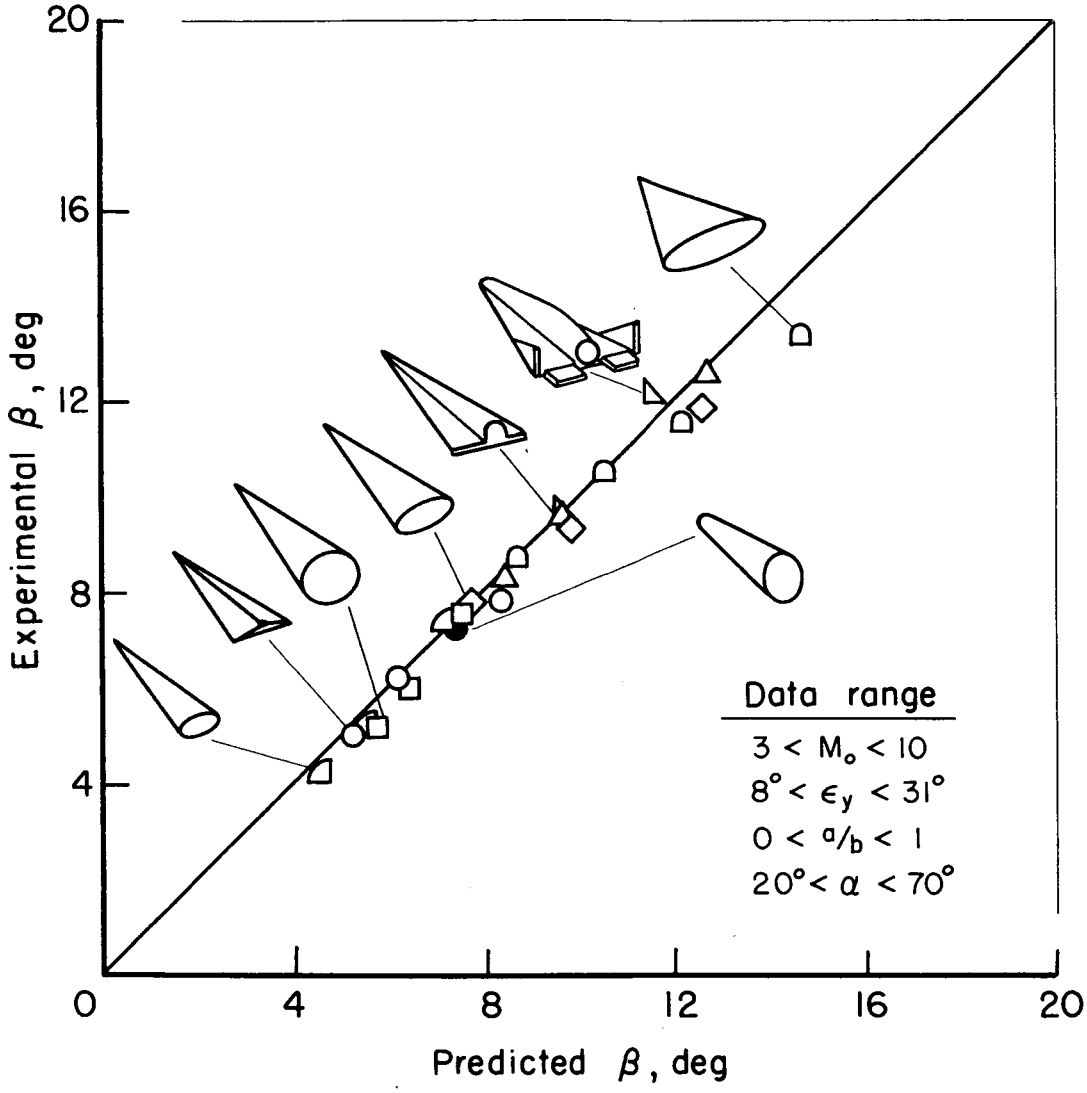

Figure 11.- Shock angles for conical vehicles at angle of attack; air.

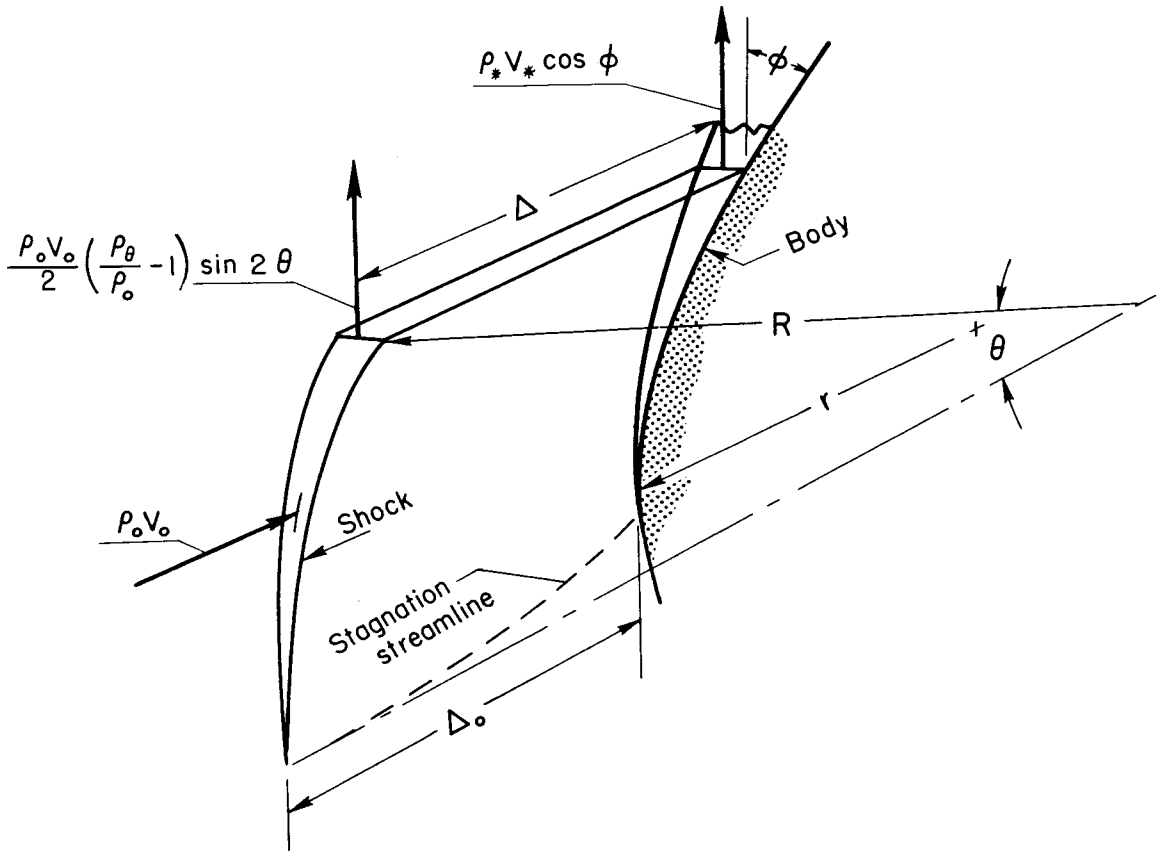

Figure 12.- Flow-continuity considerations for capsule-type vehicles.

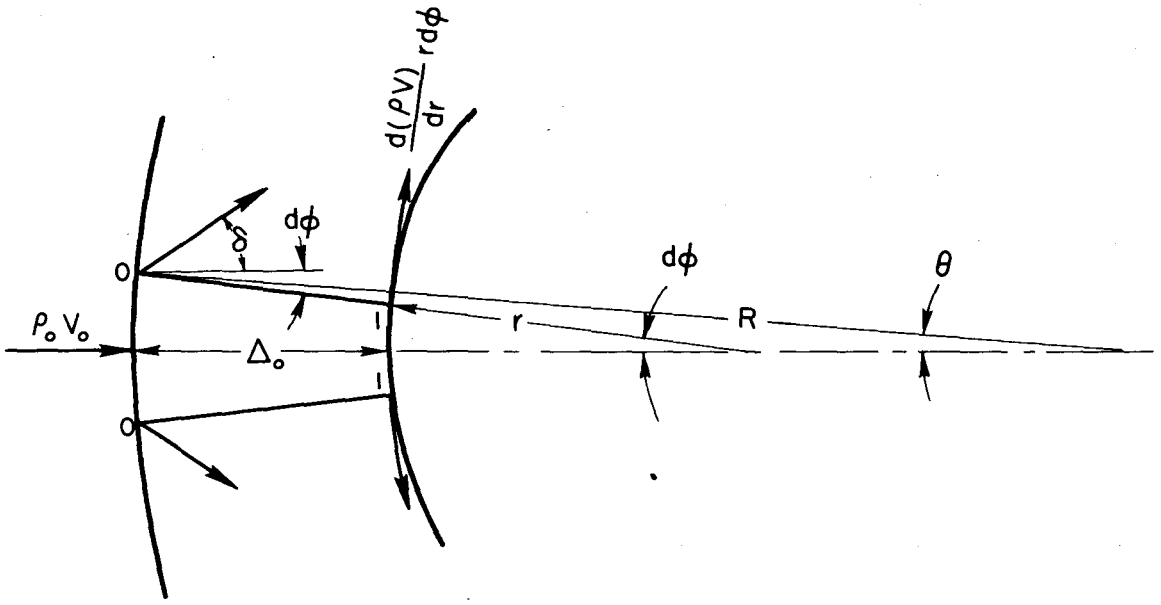

Figure 13.- Flow continuity near stagnation streamline.

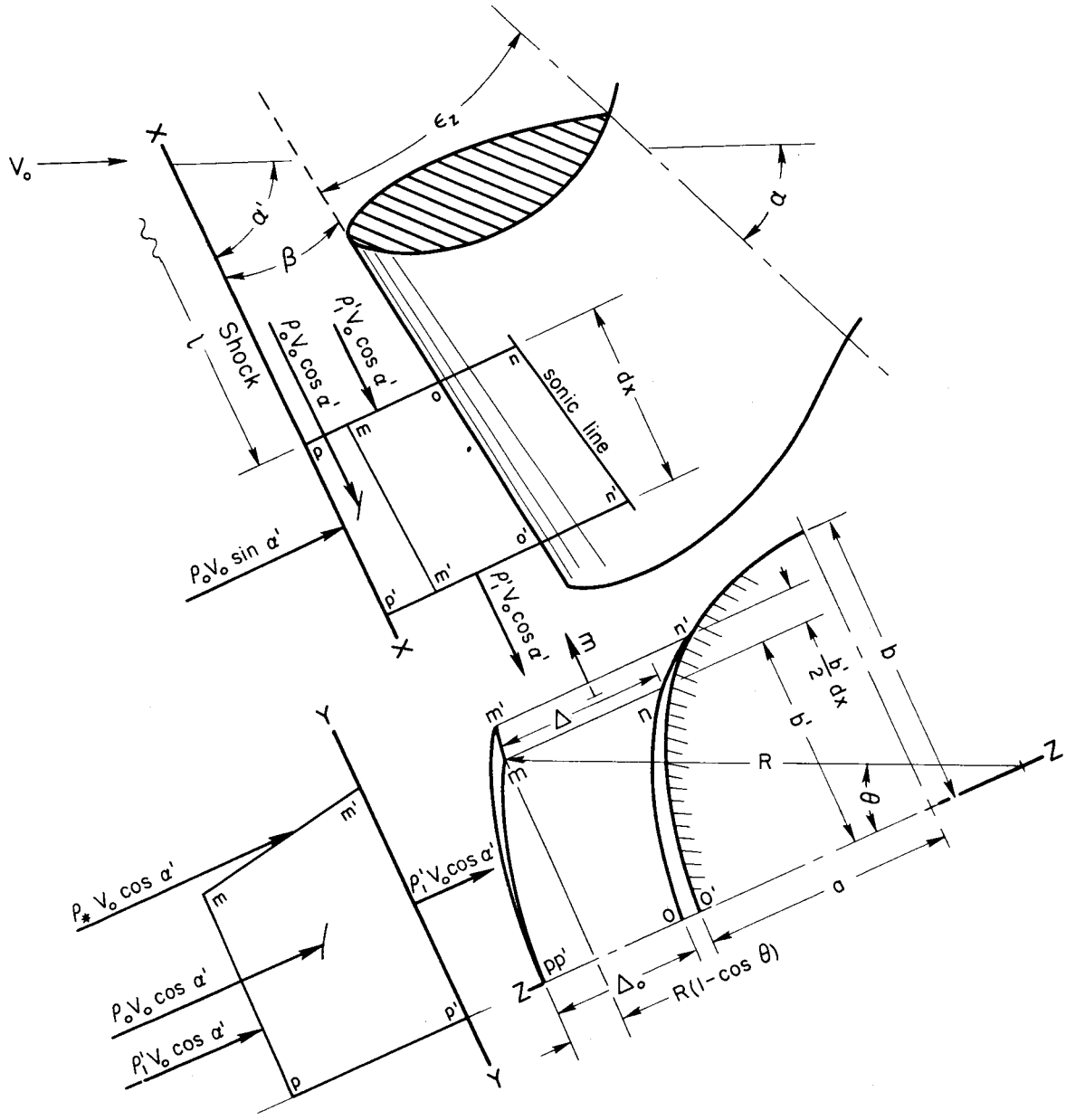

Figure 14.- Flow-continuity considerations for elliptic cone.